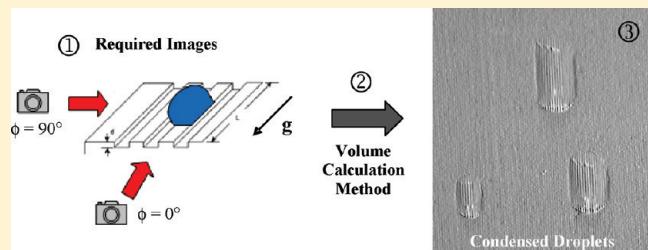# Methodology for Calculating the Volume of Condensate Droplets on Topographically Modified, Microgrooved Surfaces

A. D. Sommers*

Department of Mechanical and Manufacturing Engineering, Miami University, 56 Engineering Building, 650 East High Street, Oxford, Ohio 45056, United States

ABSTRACT: Liquid droplets on micropatterned surfaces consisting of parallel grooves tens of micrometers in width and depth are considered, and a method for calculating the droplet volume on these surfaces is presented. This model, which utilizes the elongated and parallel-sided nature of droplets condensed on these microgrooved surfaces, requires inputs from two droplet images at $\phi = 0°$ and $\phi = 90°$—namely, the droplet major axis, minor axis, height, and two contact angles. In this method, a circular cross-sectional area is extruded the length of the droplet where the chord of the extruded circle is fixed by the width of the droplet. The maximum apparent contact angle is assumed to occur along the side of the droplet because of the surface energy barrier to wetting imposed by the grooves—a behavior that was observed experimentally. When applied to water droplets condensed onto a microgrooved aluminum surface, this method was shown to calculate the actual droplet volume to within 10% for 88% of the droplets analyzed. This method is useful for estimating the volume of retained droplets on topographically modified, anisotropic surfaces where both heat and mass transfer occur and the surface microchannels are aligned parallel to gravity to assist in condensate drainage.

INTRODUCTION

The effective removal of water droplets from heat transfer surfaces is important to the overall performance of air-conditioning and refrigeration systems. In air-cooling applications, water retention on the heat transfer surface is problematic because it can reduce the air-side heat transfer coefficient, increase the core pressure drop, and provide a site for biological activity. In refrigeration systems, the accumulation of frost on the heat exchanger requires periodic defrosting and attendant energy expenditures. When water is retained on these surfaces following the defrost cycle, ice is more readily formed in the subsequent cooling period, and such ice can lead to shorter operational times between defrost cycles. Understanding the shape and size of a water droplet adhered to a surface is the key to understanding droplet retention on a surface.

The objective of this work was to devise a method for predicting the volume of a water droplet that has condensed onto a microgrooved heat transfer surface using only a few simple parameters that can be gleaned from two droplet images—a frontal image and a side image. A method for accurately calculating the droplet volume is a necessary aspect of water retention modeling and droplet distribution functions. Thus, the engineering value of this research rests in its direct application to the modeling and control of condensate on heat transfer surfaces used in dehumidification and air-cooling systems. This work also provided a better understanding of the anisotropic wettability of a highly controlled surface microstructure which might facilitate new surface designs with improved liquid drainage behavior. As part of an effort to provide guidance for the design of these

surfaces, the applicability of current models, tacitly based on an assumption of isotropic wetting, and their ability to provide reliable prediction of water droplet volume on these new surfaces was also evaluated. Because droplet shapes on surfaces with anisotropic wetting behavior are different from those on conventional, isotropic surfaces, existing models were observed to be either inadequate or less accurate.

LITERATURE REVIEW

In an early theoretical study of the effect of surface heterogeneity on the contact angle of stripwise patterned surfaces, Neumann and Good found that, for line widths below about 0.1 μm, the amplitude of the periodic contortion of the three-phase contact line is less than about 1 nm, which is indistinguishable from a straight line.[1] Therefore, at these scales, the roughness should not affect the hysteresis, and anisotropic wetting should not occur. This proposition was later supported by the theoretical work of Schwartz and Garoff which examined the capillary rise and resulting anisotropic wetting of vertical, doubly periodic patterned surfaces using energy-minimization techniques.[2] In a study of droplets on a grooved substrate, Oliver, Huh, and Mason examined droplets of polyphenylether (PPE) and mercury on parallel-grooved nitrocellulose surfaces and found that the mercury droplets were nearly spherical while the PPE droplets were cylindrical.[3] Using a mechanistic approach, Oliver and co-workers showed that the

Cassie—Baxter equation was not valid for the case of cylindrical droplets on these parallel-grooved surfaces and developed a new expression for the apparent contact angle from a two-dimensional force balance.

Morita et al. offered insight into the anisotropic wetting of micropatterned (fluoroalkyl)silane monolayer surfaces with alternating hydrophilic/hydrophobic lines of width $1-20$ μm.[4] They observed that the static and dynamic contact angles of a droplet oriented orthogonally to the stripes were $10-30°$ larger than those of the droplet oriented parallel to the stripes. Sliding angle data showed low tilt angles for droplets sliding parallel to the stripes, but droplets sliding orthogonally to the stripes resisted tilt angles of more than $80°$.

Yoshimitsu et al. studied the sliding behavior and contact angle variation of water droplets on hydrophobic pillar and groove structures prepared from a silicon wafer by dicing it and then coating it with (fluoroalkyl)silane.[5] They found that the dependence of the sliding angle on the weight of the water droplet was smallest for the parallel direction in the groove structure, followed by the pillar structure, and finally by the orthogonal direction in the groove structure. The only paper identified that addresses the condensation of water vapor onto a superhydrophobic grooved surface is the work of Narhe and Beysens.[6] In this work, silicon substrates were prepared using the same technique outlined by Yoshimitsu et al. and treated by silanization. The contact angles were $130° \pm 2°$ and $110° \pm 2°$ in the directions orthogonal and parallel to the groove, respectively.

In another related work, Chen et al. examined the apparent contact angle and shape of water droplets on parallel-grooved surfaces using both numerical and experimental approaches.[7] Equilibrium drop shapes were predicted numerically by minimizing the system free energy while simultaneously constraining the droplet volume to a fixed value. Both the initial droplet shape and the number of occupied channels were specified as inputs. It was found that multiple equilibrium shapes were possible, and the final predicted shape depended largely upon the number of channels on which the droplet resided. The apparent contact angle viewed along the channels was typically larger than the contact angle viewed perpendicular to the channels. This behavior, attributed to the pinning of the droplet against the pillars, was observed both numerically and experimentally. In their model, the droplet volume, contour shape, and contact angle are all needed a priori in arriving at the equilibrium droplet shape.

Dussan V. and Chow studied static droplet shapes at critical conditions on an inclined surface for a droplet contact line with straight-line segments on the sides.[8] In this view, the droplet was assumed to be elongated and parallel-sided. This analysis, however, was valid only in the limit of small contact angles, and Dussan V. later extended this work to allow for larger contact angles.[9] The model provided closed-form expressions for the maximum volume, speed, and wetted area of a droplet on a surface of inclination, α, but it required knowledge of the advancing and receding contact angles, θ_A and θ_R, as well as the slope of the contact angle with respect to the speed of the contact line, κ_R and κ_A. The most limiting restriction of this analysis was its assumption of small contact angle hysteresis. Observations of droplets on surfaces with microetched grooves (such as those in this work) indicate that the hysteresis can sometimes be large. Dussan V. later included the effects imposed by the motion of the surrounding fluid, but again the analysis was limited to droplets with small contact angles and small hysteresis.[10]

Briscoe and Galvin studied the critical volume of sessile and pendant droplets and found that the critical surface inclination angle, α_c, scaled with $V^{-2/3}$ for sessile droplets, where V is the volume of the droplet at incipient motion.[11] They compared their data to the prediction of maximum volume given by Dussan V. and reported reasonable agreement.[9] In a finite element solution of the Young—Laplace equation, Brown et al. were able to solve for the shape of droplets on various surfaces of inclination.[12] Their analysis did acknowledge the variation of the contact angle around the base contour, but it only considered the case of a circular base contour and predicted the horizontal contact angle, θ_H, to be intermediately located between the maximum and minimum contact angles of the drop, a behavior counter to experimental observations. Their approach, which required the specification of the tilt angle and base contour radius, also assumed that the droplet volume was known a priori.

Extrand and Kumagai studied contact angle hysteresis, droplet shape, and the retentive force for water and ethylene glycol droplets at the critical condition on polymer and silicon surfaces using a tiltable plane.[13] They found that surfaces with large contact angle hysteresis produce more elongated drops. In a numerical study of droplets at the critical condition, Dimitrakopoulos and Higdon solved for the droplet configuration that produced minimum contact angle hysteresis (i.e., $\theta_A - \theta_R$) for a specified advancing angle θ_A and Bond number.[14]

Other relevant works include those of Merte and Son and Merte and Yamali, who studied the equilibrium shape and departure size of two-dimensional dropwise condensation on a vertical surface.[15,16] A model was developed which minimized the total energy of the droplet using techniques from variational calculus. Simulation results were compared against experimental data, with reasonable agreement found. In this two-dimensional model, however, the volume was specified a priori. Moy et al. developed a modified axisymmetric droplet shape analysis approach, ADSA-MD (maximum diameter), to measure the contact angles of nonwetting droplets from top-view images of the droplet.[17] In this numerical technique, the maximum diameter and droplet volume are both specified as input parameters in addition to fluid properties.

In two recent reports by El Sherbini and Jacobi, droplet shapes were studied experimentally.[18,19] The droplet shape was approximated using a "two-circle method" in which the droplet profile is fitted with two circles sharing a common tangent at the apex of the droplet. The volume was then calculated by integrating the profile around the circumference of the base. This method was found to accurately predict the volume of droplets, knowing only the contact angle and shape of the three-phase contact line. Their work was developed for conventional surfaces of homogeneous roughness. In the work of El Sherbini and Jacobi, the base contour was assumed to be elliptical and continuous. Observations of droplets on surfaces with microetched grooves indicate that this modeling approach used on conventional surfaces does not readily extend to topographically anisotropic surfaces.

Other germane studies include those by Amirfazli and co-workers—Amirfazli et al., Bateni et al., Li and Amirfazli, and Antonini et al.[20−23] In these later works, various methods are described for high-accuracy contact angle measurements (i.e., a polynomial fitting scheme, a thermodynamic approach, and a drop shape analysis algorithm (ADSA-TD) that uses two sessile drops). In the most recent work, an image-based adhesion force analysis (IBAFA) methodology is described that reconstructs the contact line shape using a Fourier cosine series and evaluates the
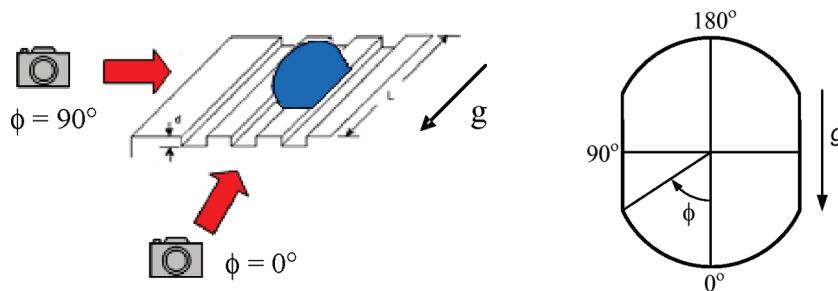
Figure 1. Contact angle measurement configuration with channels oriented parallel to gravity.

adhesion force. It is important to note that while this method can handle irregular droplet shapes (i.e., noncircular and none-lliptical) such as those arising on surfaces with an anisotropic topography, multiple droplet profile images are required and the droplet volume is not explicitly calculated.

In summary, understanding the behavior, shape, and size of water droplets is the key to understanding droplet retention on a surface. Significant research has already been reported on analytical and numerical methods for calculating the droplet volume on smooth surfaces as well as homogeneously rough surfaces. However, no calculation method was found that specifically addresses the volume calculation of condensed water droplets on parallel, microgrooved surfaces. The inability of existing models to satisfactorily calculate the droplet volume is largely ascribed to the unusual variation of the apparent contact angle around the base of the drop, the discontinuity of the three-phase contact line, and the elongated, parallel-sided droplet shape. Therefore, if functional topography is to be useful as a method for manipulating wettability for the purpose of controlling condensation or water drainage on heat transfer surfaces, then new models and calculation methods are needed.

■ BACKGROUND AND METHODOLOGY

The contact angle θ that a liquid droplet forms on a horizontal surface is described by the classical equation by Young (1855)

$$\cos \theta = \frac{\gamma_{SV} - \gamma_{SL}}{\gamma_{LV}} \quad (1)$$

where γ_{SV}, γ_{SL}, and γ_{LV} are the interfacial free energies per unit area of the solid–vapor, solid–liquid, and liquid–vapor interfaces, respectively.[24] The specific contact angle that a water droplet forms on a surface has long been used as a gauge of the hydrophobicity of the surface. However, depending on how the water droplet forms on a rough surface, at least two different wetting regimes can exist. The first form, known as the "wetted surface", occurs when the water droplet completely fills the surface asperities. This particular wetting regime, which may result from melting frost or condensing water vapor, is usually described by Wenzel's theory of wetting (1936) such that

$$\cos \theta' = r \cos \theta \quad (2)$$

where θ' is the apparent contact angle of the droplet wetting the surface and r is the surface roughness factor defined as the ratio of the actual wetted area to the geometric projected area.[25] This ratio always has a value greater than or equal to unity. The second type known as the "composite surface" occurs when the droplet is suspended over the asperities, leaving air trapped beneath it. This form of wetting frequently occurs when the droplet is injected by syringe onto a surface having sufficiently small surface features. Composite surfaces are described by

Cassie–Baxter's theory of wetting (1944), where

$$\cos \theta' = -1 + \varphi(\cos \theta + 1) \quad (3)$$

and φ represents the surface area fraction of the wetted area to the projected area.[26] This fraction always has a value less than unity. By themselves, however, large contact angles associated with a hydrophobic surface do not ensure that a surface easily sheds water. Therefore, the sliding angle is also a useful criterion when evaluating the water drainage behavior of surfaces. The sliding angle is the critical angle for a water droplet of known mass to first begin sliding down an inclined surface.

The objective of this research was to develop a new general method for calculating the volume of liquid droplets on parallel-grooved metallic surfaces, and as such it was important to understand how such modeling might depend on the wetting modes described by the Wenzel and Cassie–Baxter models. To explore the Cassie–Baxter mode of wetting, a micrometer syringe (Gilmont Instruments Inc.) was used to inject droplets onto the microgrooved surface. To explore the Wenzel mode of wetting, a thermoelectric cooler was used to condense water vapor onto the test surface at fixed surface temperature and relative humidity inside an environmental enclosure using the approach described by Sommers and Jacobi.[27] The humidity was measured using a capacitive thin-film sensor, and moisture was provided by a cool-mist ultrasonic humidifier. Intermittently, a cotton swab was used to remove excess water from the surface to allow for the undisturbed growth of single isolated droplets. Once a droplet of sufficient size was grown, the droplet was imaged and then absorbed in a high-density filter paper and weighed on a high-precision electronic balance accurate to ±0.0001 g to determine its volume.

The apparent contact angles and base dimensions of the droplets were obtained using a Ramé-Hart goniometer in combination with a high-resolution charge-coupled device camera. Droplets were photographed with the etched channels aligned parallel to gravity as shown in Figure 1 with images recorded at azimuthal angles of 0° and 90°. The grooves were aligned with gravity because that configuration has been shown to be the most promising for promoting drainage. Typical uncertainty in the measured contact angle was 1–2°, while typical uncertainty in the droplet diameter was 2–3%, with the maximum uncertainty not exceeding 7%. The microgrooved surfaces were produced using standard photolithographic practices and a reactive ion etching (RIE) technique described by Sommers and Jacobi.[27] Alternatively, a wet chemical etching technique involving Transene aluminum etchant type A was also used in combination with photolithography to produce a few microgrooved surfaces. The first method (i.e., RIE etching) results in vertical sidewalls, whereas the second method (i.e., wet chemical etching) produces more rounded sidewalls as shown in Figures 2 and 3.

Parallel channels approximately tens of micrometers in width and depth, running the length of the surface, were etched into plates of aluminum alloy 1100 (99.9% pure Al), 63.5 mm by 63.5 mm by 3.2 mm in size. Aluminum was chosen because it is naturally hydrophilic and is the material of choice in many heat and mass transfer applications. The plates had an average roughness, R_a, of 25–35 nm prior to etching. After
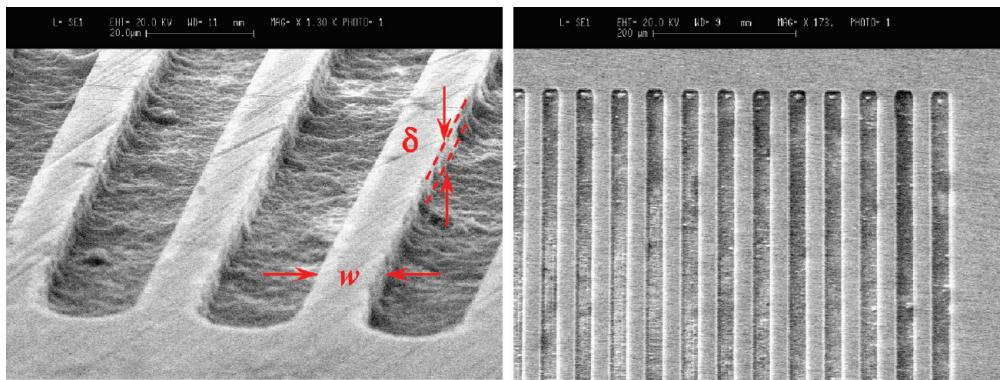
Figure 2. SEM images of sample 6 (left) having an etch depth of approximately 6.2 μm and sample 9 (right) having an etch depth of approximately 6.9 μm.

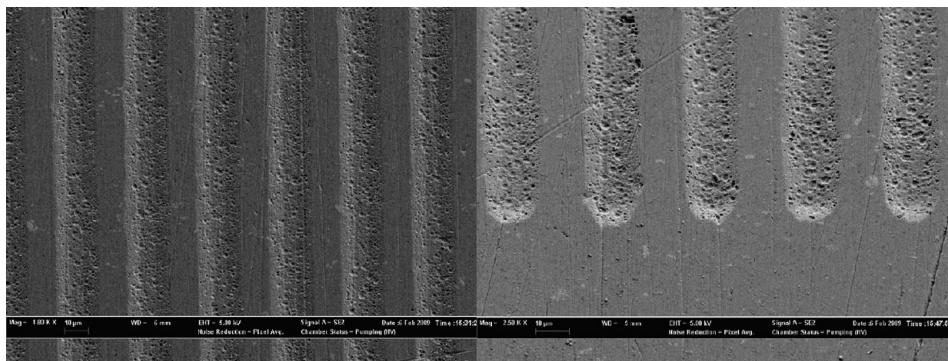**Figure 3.** SEM images of a wet-etched aluminum sample having a groove width of approximately 15 μm. The images were taken at magnifications of 1800× and 2500×, respectively.

undergoing etching, the plates were analyzed using either a Cambridge S-360 scanning electron microscope or a Zeiss Supra 35 VP FEG scanning electron microscope as well as an Alpha-Step profilometer to determine the surface geometry accurately. Scanning electron microscope images of a couple representative surfaces are included in Figures 2 and 3 A list of all manufactured surfaces can be found in Table 1. (Note: The surfaces shown in this table were all produced via reactive ion etching.)

■ NEW VOLUME CALCULATION METHOD

For the idealized case where the liquid droplet is resting on a horizontal plane, the droplet takes the shape of a spherical cap where the base contour is circular and the contact angle is constant around the base. For this special case, the calculation of the droplet volume is pretty straightforward and can be found using

$$V = \frac{\pi D^3}{24}\left(\frac{2 - 3\cos\theta + \cos^3\theta}{\sin^3\theta}\right) \quad (4)$$

where D is the diameter and θ is the contact angle. However, the accuracy of this equation quickly degenerates as the droplet elongates due to surface inclination (or perhaps the underlying surface morphology). Because droplets on these anisotropic surfaces tend to be elongated and possess a parallel-sided base contour shape, using the hemispherical cap approximation to estimate their volume can be especially problematic. The calculation of water droplet volume is important in the prediction of condensate retention on the heat transfer surface. If the volume function is known, then it could be multiplied by a droplet size-distribution function and integrated over the droplet diameters and surface area to provide an estimate of the condensate retention on a given surface.

Table 1. Etched Sample Characteristics

sample no.	pillar width, w (μm)	pillar depth, δ (μm)	aspect ratio, δ/w
1	26.8	5.2	0.194
2	25.2	15.7	0.623
3	23.2	27.0	1.174
4	13.42	13.32[a]	0.801
5	14.91	7.85	0.526
6	14.00	6.19	0.442
7	10.40	22.00[a]	1.964
8	16.05	4.97	0.310
9	19.92	6.89	0.346
10	24.90	6.89	0.277
11	38.00	6.89	0.181
12	4.62	6.89	1.490

[a] Indirect measurement.

Others have developed methods for calculating the volume of water droplets; however, most of these methods were developed for, and tacitly reply upon, droplets on homogeneous surfaces with little elongation. For instance, the "two-circle model" developed by El Sherbini and Jacobi,[19] which represents an improvement over the hemispherical cap method (i.e., single-circle method), was based on experimental observation for droplets where $\beta < 1.5$ and therefore was intended primarily for droplets with mild elongation. In the current work, the elongation of the droplet often exceeds $\beta = 2.5$, so the applicability of this method remains dubious.
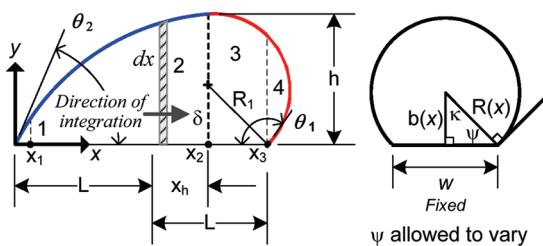
Figure 4. The droplet profile is approximated using both a circle and a teardrop shape.

Figure 5. The constants in the droplet profile equations are found by matching the contact angles and droplet height.

The purpose of this work was to provide a more reliable method for calculating the volume of a droplet as a function of its diameter and contact angles on a nonhomogeneous surface. In this new approach to calculating the water droplet volume, the droplet is treated as a cylindrical element, and the volume is found by integrating the cross-sectional area down the length of the droplet rather than by the sweeping around the periphery of the droplet and integrating droplet profiles taken at all azimuthal angles. The advantage of using this method over the two-circle method is that it utilizes the wetting behavior of droplets on these microstructured surfaces and therefore does not require a priori information about the droplet base contour shape or azimuthal contact angle variation. (Note: This information is provided as inputs in the two-circle method.) Thus, this new approach takes advantage of the unique characteristics of water droplets on these surfaces—namely, their elongated, parallel-sided base contour shape.

The idea behind this aforementioned extrusion method is relatively simple. As shown in Figure 4, the droplet is split into two regions (red and blue), each of which is then further subdivided into two smaller components. Regions 1 and 2 are fit by a teardrop profile

$$y = \frac{x}{c_1}\sqrt{c_2 - x^2} \tag{5}$$

where c_1 and c_2 represent constants to be determined later, and regions 3 and 4 are fit by a circle having the form

$$y - \delta = \sqrt{R_1^2 - (x - (L + x_h))^2} \tag{6}$$

where δ represents the height of the circle's center above the surface and x_h represents the lateral offset of the circle's center (or the x component of the distance from the midpoint of the base length to the center). (Note: The teardrop profile was chosen because for the application motivating this research (i.e., condensation on vertical fin surfaces), droplets have been observed to exhibit this profile. Other boundary profile equations, however, may be used and easily adopted in the model. For highly nonwetting droplets, using two circles to fit the profile may be preferred since the accuracy of the teardrop profile begins to degenerate for $\theta_2 > 90°$.)

In this method, the variables h, L, w, θ_1, and θ_2 are supplied by the user and everything else is calculated, including x_h. (If empirically based correlations are used, the number of user-supplied inputs can be reduced to four parameters.) The constants appearing in the teardrop profile, c_1 and c_2, are found by matching the height of the droplet, h, and the apparent contact angle, θ_2. The first boundary condition is found by taking the derivative of the teardrop function

$$\frac{dy}{dx} = \frac{1}{c_1}\sqrt{c_2 - x^2} - \frac{x^2}{c_1}\frac{1}{\sqrt{c_2 - x^2}} \tag{7}$$

The slope is then related to the contact angle by

$$\left.\frac{dy}{dx}\right|_{x=0} = \tan\theta_2 = \frac{\sqrt{c_2}}{c_1} \tag{8}$$

which is the first specified boundary condition. The second boundary condition is found by specifying the height of the droplet and
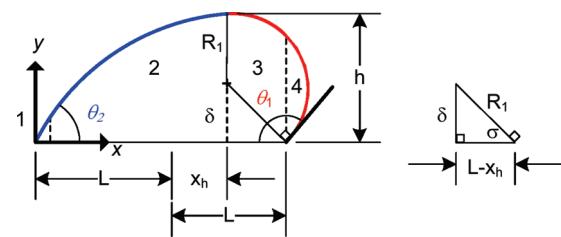
substituting $x = L + x_h$ into the original function, eq 5, to get

$$h = \frac{L + x_h}{c_1}\sqrt{c_2 - (L + x_h)^2} \tag{9}$$

The constants in the circular profile, δ and R_1, are found similarly by matching the droplet height h and contact angle θ_1 with the specified inputs. The height is fixed by recognizing that

$$h = R_1 + \delta \tag{10}$$

and the contact angle is fixed according to

$$\cos\sigma = \frac{L - x_h}{R_1} \quad \text{where} \quad \sigma = \theta_1 - \frac{\pi}{2} \tag{11}$$

as shown in Figure 5.

The actual process of extruding a circular cross-sectional area through regions 2 and 3 is accomplished as follows:

$$V_{\text{total}} = V_1 + V_2 + V_3 + V_4 \tag{12}$$

where

$$V_2 = \int_{x_1}^{x_2} A_c \, dx \quad \text{and} \quad V_3 = \int_{x_2}^{x_3} A_c \, dx \tag{13, 14}$$

where $x_1 = \varepsilon$ (for $\varepsilon \ll 1$), $x_2 = L + x_h$, and $x_3 = 2L$ as shown in Figure 4. The area of the extruded circular segment is equal to the area of the circular sector minus the area of the triangular portion such that

$$A_c = \frac{[R(x)]^2}{2}(\theta - \sin\theta) \tag{15}$$

where $R(x)$ is the radius of the extruded circle which is a function of the distance along the x coordinate and θ is the central sector angle. If θ is bisected so that $\theta = 2K$ such as shown in Figure 4, then this can be rewritten such that for wetting droplets

$$A_c = \frac{[R(x)]^2}{2}(2\kappa - \sin 2\kappa) \tag{16}$$

and for nonwetting droplets

$$A_c = \pi[R(x)]^2 - \frac{[R(x)]^2}{2}(2\kappa - \sin 2\kappa) \tag{17}$$

The volume of region 1 (i.e., V_1), which is typically less than 0.5% of V_{total}, is approximated using the volume formula for a triangular prism, yielding

$$V_1 \approx \frac{1}{2}\varepsilon\left(\frac{\varepsilon}{c_1}\sqrt{c_2 - \varepsilon^2}\right)\left(\frac{L}{\beta}\right) \tag{18}$$

The volume of region 4 (i.e., V_4), which is typically less than 1% of V_{total}, is found using the volume formula for a spherical cap, which after substitution yields the following result:

$$V_4 = \frac{1}{6}\pi y_c(3r_c^2 + y_c^2) \tag{19}$$

Table 2. Volume Comparison for the Extrusion, Two-Circle, and Spherical Cap Methods

n	$\theta_{\min}$ (°)	θ_{adv} (°)	L (mm)	w (mm)	h (mm)	volume (μL), new method	volume (μL), two-circle method	volume (μL), spherical cap method (D_{eq})
1	50	80	6.5	5.5	1.752	31.46	29.89	30.36
2	55	80	6.5	5.0	1.67	28.22	27.90	27.93
3	45	50	6.5	5.0	1.10	17.78	17.24	17.04
4	45	50	6.5	5.5	1.21	21.65	19.74	19.66
5	45	50	6.5	5.75	1.265	23.71	21.05	21.01
6	60	65	7.0	5.0	1.517	28.20	28.27	27.70
7	60	65	7.0	5.25	1.593	31.24	30.25	29.80
8	60	65	7.0	5.5	1.669	34.43	32.29	31.96
9	60	65	7.0	5.75	1.745	37.75	34.39	34.16
10	60	65	7.0	6.0	1.82	41.19	36.55	36.41
11	60	65	7.0	6.25	1.896	44.79	38.78	38.71
12	35	40	5.0	4.5	0.7638	8.295	7.39	7.39
13	35	40	5.0	4.25	0.7213	7.385	6.80	6.78
14	35	40	5.0	4.0	0.6789	6.520	6.24	6.19
15	35	40	4.0	3.5	0.594	4.007	3.63	3.63
16	35	40	4.0	3.25	0.5516	3.443	3.26	3.24
17	75	80	8.0	6.0	2.408	68.25	64.62	63.66
18	75	80	8.0	5.5	2.207	56.81	57.32	55.87
19	35	80	6.5	6.25	1.714	29.78	28.91	30.69
20	35	80	6.5	6.0	1.646	27.63	27.16	28.87
21	40	80	6.5	6.25	1.804	33.25	31.28	32.61
22	45	80	6.5	6.25	1.896	36.83	33.66	34.64
23	30	50	6.5	6.5	1.183	22.03	20.05	20.49
24	30	55	6.5	6.5	1.264	23.01	21.36	22.03
25	30	65	6.5	6.5	1.43	25.04	24.02	25.26
26	30	70	6.5	6.5	1.515	26.18	25.38	26.97

where y_c refers to the height of the cap and r_c refers to the radius of the circle that forms the base of the cap.

The local cross-sectional radius $R(x)$ is related to the local droplet height $y(x)$ by the following expressions as shown in Figure 4:

$$y = R(x) + b(x) \tag{20}$$

where

$$R(x) = \frac{w}{2\cos\psi} \quad \text{and} \quad b(x) = \frac{w\tan\psi}{2} \tag{21, 22}$$

Because these functions vary with the x coordinate and the droplet width w is fixed by the surface microstructure, the angle ψ is allowed to vary with the x coordinate, which allows this method to also be used to predict the maximum contact angle occurring along the side of the droplet at $x = L + x_h$ as will be shown later. Finally, using the Young–Laplace equation, the location x_h where the droplet height in the y direction is maximum can be found using

$$x_h = \frac{-a_3 + \sqrt{a_3{}^2 - 2a_1 a_2}}{a_1} \tag{23}$$

where

$$a_1 = (\rho_l - \rho_v)g/\gamma \tag{24}$$

$$a_2 = \frac{1}{2}\left(\sin\theta_1 - \sin\theta_2 - (\rho_l - \rho_v)gL^2/\gamma\right) \tag{25}$$

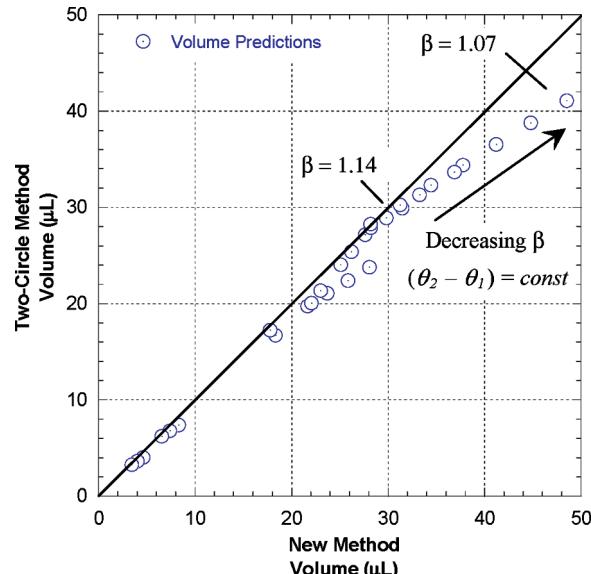$$a_3 = (\sin\theta_1 + \sin\theta_2)/2L \tag{26}$$

Figure 6. Effect of the elongation ratio β on the new calculation method as compared with the two-circle method.

■ RESULTS AND DISCUSSION

The new method was initially compared to the two-circle method developed by El Sherbini and Jacobi[19] and the hemispherical cap
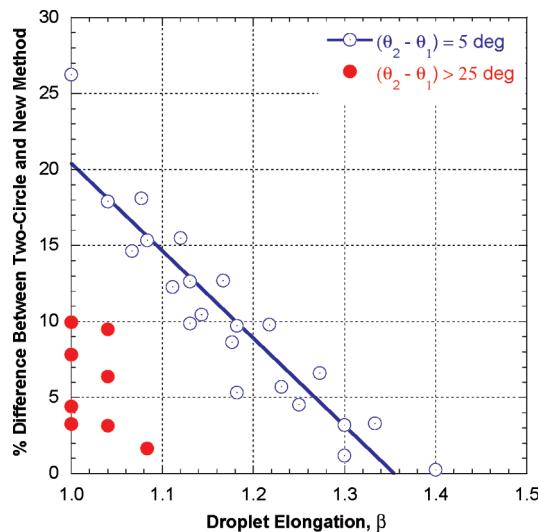
Figure 7. Effect of the contact angle hysteresis on the new calculation method as compared with the two-circle method.
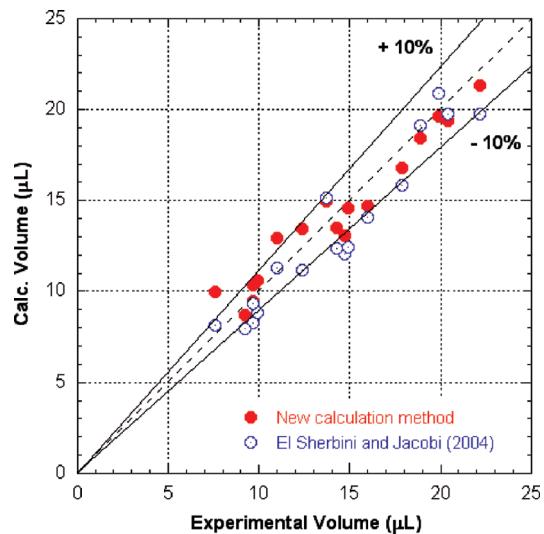

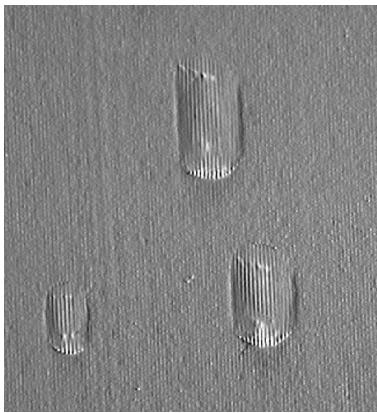**Figure 9.** Comparison of the two-circle and extrusion-based droplet volume calculation methods.

Figure 8. Images of condensed droplets on a microgrooved surface exhibiting the elongated, parallel-sided base contour shape.

Figure 10. A 10 μL composite droplet image illustrating the five required inputs to the model.

Table 3. New Method Compared to Experimental Data

experimental volume (μL)	calculated volume (μL)	difference (%)
19.90	19.63	1.36
9.70	9.48	2.27
14.70	13.08	11.0
22.20	21.35	3.83
17.90	16.81	6.09
14.30	13.51	5.52
9.90	10.63	7.37
14.90	14.56	2.28
12.40	13.46	8.55
9.20	8.68	5.65

approximation (eq 4) by calculating the volume of synthetic droplets of arbitrarily specified parameters (i.e., θ_1, θ_2, L, w, h). Various droplet lengths and contact angles ($n = 26$) were examined to check for any potential problems associated with using the new method (see Table 2.) For these comparisons, the same geometry
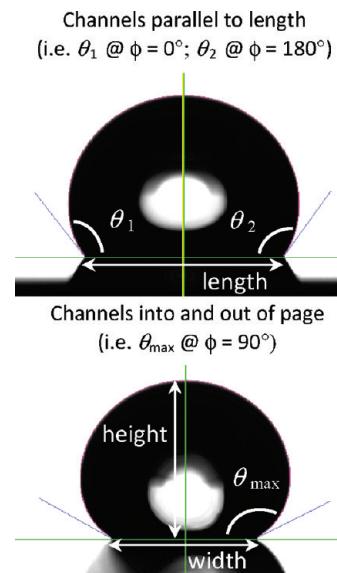
and contact angle information was provided to each method. For the hemispherical cap approximation, the equivalent diameter D_{eq} and average contact angle were used (i.e., $(\theta_1 + \theta_2)/2$). From this initial comparison, a few interesting observations were made. First, although the true droplet volume is not known in this comparative approach, the new method did predict slightly higher droplet volumes on average than either of the other two methods. For $\beta > 1.0$, the new extrusion-based method yielded slightly higher droplet volumes than the two-circle method in all cases except two. The largest difference between these two methods was +15.5%. Droplet volumes calculated using the new method, however, differed from the hemispherical cap approximation more uniformly on both sides—namely, from −4.4% to +15.7%. These differences can be attributed to the droplet height, which was held the same in all cases. The new extrusion-based method is proposed for use

on microgrooved surfaces where droplet elongation is observed and the droplet height would be diminished slightly relative to the homogeneous surface due to this elongation of the droplet. Thus, since the same droplet height was supplied to each method in this comparison, the new method would be expected to predict slightly larger droplet volumes.

A second observation involved the effect of the droplet elongation, β, on the calculated volumes using these three approaches. As shown in Figures 6 and 7, the two methods showed the most agreement when the droplet elongation was
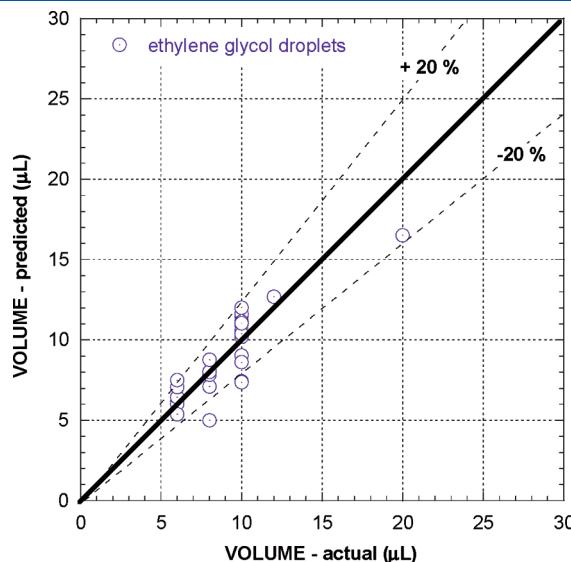

Figure 11. Accuracy of the new calculation method when applied to injected ethylene glycol droplets.

pronounced (i.e., $\beta > 1.2$). In contrast, the difference between the two-circle method and the new extrusion-based calculation method was most significant for small β. This observation is consistent with the original development and intended application of the new method—namely, parallel-sided, *elongated* droplets. As seen in Figure 7, the percent difference between these two methods was directly commensurate with the elongation of the droplet. The extent of the difference, however, depends on the contact angle hysteresis (or $\theta_2 - \theta_1$). When the contact angle difference is large, the new method is better able to handle small β values. This is also consistent with the droplet profile shapes used in this new method—namely, the teardrop shape and the circular shape, which when used together better match the shape of a droplet when the contact angle hysteresis is large. On the basis of these findings, the new extrusion-based method is recommended for $\beta > 1.2$ when $\theta_2 - \theta_1 < 25°$ and for $\beta < 1.2$ when $\theta_2 - \theta_1 \geq 25°$.

Next, these ranges of proposed applicability were examined by comparing droplet volumes calculated using this new method against experimental data of actual condensed and injected droplets. For water droplets condensed on these microstructured surfaces (see Figure 8), the new method yielded an accuracy that was similar to, or better than, that of the two-circle method. A comparison between these two methods is shown in Table 3 and graphically in Figure 9. It should be pointed out that these experimental droplet volume data represent water droplets condensed on sample 2 and therefore the Wenzel mode of wetting. These volume data were determined by the absorption and subsequent direct weighing of the droplet on a high-precision balance, and as a result, these experimental data are not as accurate as those obtained using a microsyringe. The maximum uncertainty of the experimental data was $\pm 0.5\ \mu L$. Nonetheless, Figure 9 highlights the ability of this new method to

Table 4. Maximum Contact Angle Prediction

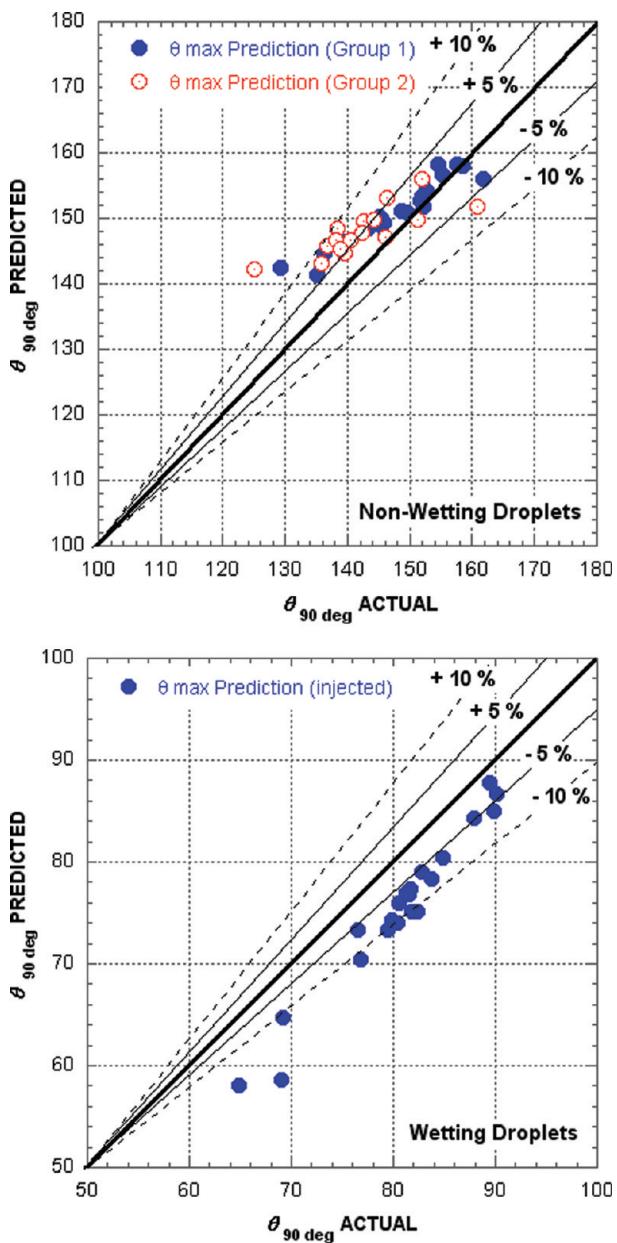|	nonwetting droplets (water)							wetting droplets (EG)						
n	θ_1 (°)	θ_2 (°)	L (mm)	W (mm)	h (mm)	measured angle	new method	n	θ_1 (°)	θ_2 (°)	L (mm)	W (mm)	h (mm)	measured angle	new method
1	116.4	111.9	3.839	2.652	2.496	145.1	150.2	1	44.8	43.8	10.894	4.634	1.299	69.0	58.55
2	113.2	111.2	4.342	2.581	2.722	152.0	153.3	2	47.6	45.7	8.961	4.929	1.366	64.8	58.0
3	116.4	114.1	4.231	2.998	2.689	145.5	148.9	3	45.7	45.6	6.629	2.737	1.116	83.7	78.39
4	103.2	100.8	5.492	3.076	2.856	145.4	149.9	4	48.3	45.3	6.616	2.933	1.128	81.8	75.13
5	120.0	118.4	4.277	2.903	2.797	149.7	150.9	5	47.3	45.3	6.595	3.213	1.019	69.2	64.77
6	112.6	109.5	4.582	2.955	2.695	145.8	149.3	6	49.4	48.1	6.026	3.063	1.08	76.8	70.38
7	109.8	106.8	4.385	2.346	2.750	161.7	155.9	7	46.9	46.0	5.634	2.272	0.904	81.3	77.02
8	116.4	112.0	4.606	3.116	2.758	143.3	148.5	8	50.0	48.3	4.479	2.557	0.964	80.4	74.03
9	119.4	117.5	4.161	3.426	2.693	136.2	144.7	9	51.6	49.4	6.537	2.849	1.095	82.4	75.1
10	110.4	109.6	5.233	3.385	2.845	138.7	146.9	10	49.3	47.4	6.053	2.481	0.969	80.5	75.99
11	106.9	106.9	3.880	2.219	2.434	152.6	154.3	11	46.2	45.5	6.665	2.663	1.065	81.7	77.31
12	112.1	107.7	4.487	2.635	2.701	151.6	152.6	12	48.2	47.8	6.828	2.778	1.035	76.5	73.38
13	117.1	113.8	4.373	2.898	2.811	148.6	151.1	13	51.4	50.1	4.981	2.254	0.889	81.6	76.53
14	102.6	102.3	3.374	1.773	2.139	155.2	156.6	14	50.8	49.5	5.714	2.074	0.978	90.2	86.65
15	105.7	105.6	3.222	1.631	2.119	157.5	158.2	15	50.6	48.4	5.674	2.350	0.994	84.8	80.46
16	103.6	102.2	3.638	1.709	2.198	158.6	158.0	16	50.3	49.2	5.716	2.632	0.997	79.8	74.3
17	95.5	95.3	2.899	1.328	1.723	154.6	158.2	17	52.7	51.9	6.115	3.121	1.161	79.5	73.3
18	94.4	92.3	7.003	3.971	2.920	129.3	142.4	18	47.2	46.7	7.509	2.761	1.139	82.8	79.05
19	100.7	100	6.358	4.139	2.945	135.2	141.3	19	49.5	48.9	6.239	2.187	1.052	89.4	87.78
								20	50.1	49.7	5.795	2.268	1.026	87.9	84.28
								21	53.3	50.5	6.733	2.527	1.157	89.9	84.96

Figure 12. The new calculation method was shown to predict the maximum contact angle of both nonwetting droplets and wetting droplets to a high level of accuracy.

determine the droplet volume using a few measured geometrical parameters and compares these results to the two-circle method developed by El Sherbini and Jacobi.[19] It should be noted that, for these data, the two-circle method generated 11 cases where the percent error was greater than or equal to 10%. By comparison, this new extrusion-based technique only produced four cases where the percent error equaled or exceeded 10%. Because water droplets on these microstructured surfaces tend to be parallel-sided and are often highly elongated, this method appears to hold tremendous promise as a nonintrusive means of determining the droplet volume. It requires only a few simple inputs which can be gleaned from two images of the droplet at ϕ = 0° and ϕ = 90°—namely, the droplet major axis, minor axis, height, and apparent contact angles at both the advancing and receding fronts of the droplet. It should be noted, however, that this new method of finding the droplet volume tacitly relies upon the parallel-sided nature of these droplets and as a result is not intended for droplets on conventional surfaces possessing an elliptical base contour shape.

The volume of injected droplets was also studied using the new calculation method. For these tests, a micrometer syringe (Gilmont Instruments Inc.) was used to inject droplets, 10−50 μL in size, onto the surface. The maximum uncertainty of these data was ±0.25 μL. These data were collected by examining 22 different composite water droplets on sample 5 such as the one shown in Figure 10. Because these droplets did not fully wet the microchannels, the parallel-sided base contour shape of the droplets was not fully realized. As a result, this new method for calculating the droplet volume tended to underpredict the droplet volume. For these droplets, the average error associated with using this method was 15.6% whereas the average error associated with using the two-circle method was 13.2%. Thus, for droplets departing from the parallel-sided base contour shape, the two-circle method developed by El Sherbini and Jacobi[19] provides slightly more accurate results. (Note: In the original two-circle method, height is not specified as an input parameter. Thus, to ensure a fair comparison, the two-circle method was modified slightly to include height as an independent variable. In this way, both methods started with the same specified inputs.)

The new method was also applied to ethylene glycol droplets injected onto the surface using a micrometer syringe. Ethylene glycol, which is a common heat transfer fluid, was examined to test the generality of the new volume calculation method. For a sample size of n = 29 droplets, the average error was 11.7% (see Figure 11). Because the surface tension for ethylene glycol/air is smaller than that for water/air, the droplet was generally more elongated and often extended outside the field of view of the camera. Thus, an additional image was required to measure the length of the major axis of the droplet, which introduced error into the calculation method. Nonetheless, these data support the overall accuracy and generality of the proposed method.

The maximum contact angle of liquid droplets on micro-grooved surfaces can also be predicted using this new calculation methodology. Because the contact line is "pinned" on the sides due to the presence of the channels, the maximum apparent contact angle typically occurs at ϕ = 90° on these surfaces instead of at ϕ = 0° (i.e., the advancing front) as is common on isotropic surfaces. This interesting phenomenon, which can be seen in Figure 10, has been observed at various angles of surface inclination as well as for various droplet volumes.[28] This phenomenon, which is not present on isotropic surfaces, is manifest for both wetting and nonwetting droplets (see Table 4). For these experiments, the nonwetting (or composite) droplets were formed using water, while the wetting droplets were formed using ethylene glycol. For the nonwetting droplets, the new method predicted the measured contact angle occurring at ϕ = 90° on average to within 2.9% for n = 19 droplets, and for the wetting droplets, the new method predicted the actual maximum contact angle on average to within 6.6% for n = 21 droplets as shown in Figure 12. By contrast, the two-circle method assumes that θ_{max} = θ_1. For the data shown in Table 4, however, the measured θ_{max} can actually be up to 45% higher than θ_1 due to contact line pinning. Thus, this new method provides a better prediction of the maximum angle and therefore a better model of the anisotropic wettability of a highly controlled surface microstructure. (Note: The two-circle method was developed for homogeneous surfaces and was never

intended to be applied to anisotropic surfaces.) Herein lies the value of the new method. In addition to the improved accuracy of the calculated droplet volume, the new method may be used to accurately predict the maximum droplet contact angle that occurs on these surfaces at $\phi = 90°$. Because it provides a better model of the wetting characteristics of these surfaces, it could be used to facilitate the design of more robust, anisotropic water-shedding surfaces. Such surfaces could have profound implications in a range of engineering applications. Furthermore, methods for accurately calculating the droplet volume are a necessary aspect to water retention modeling and droplet distribution functions. Thus, the engineering value of this research rests in its direct application to the modeling and control of condensate on heat transfer surfaces used in dehumidification and air-cooling systems.

■ CONCLUSIONS

A method for calculating the volume of liquid droplets on anisotropic, microgrooved surfaces is presented. This method, which utilizes the elongated and parallel-sided nature of liquid droplets on these surfaces, uses inputs from two different droplet images at $\phi = 0°$ and $\phi = 90°$—namely, the droplet major axis, minor axis, height, and two contact angles. In this method, a circular segment of varying height is extruded the length of the droplet where the chord length of the segment satisfies the width requirement of the droplet. The new extrusion-based method is recommended for droplet aspect ratios $\beta > 1.2$ and for $\beta < 1.2$ when $\theta_2 - \theta_1 \geq 25°$ and is most accurate when $\theta_2 < 90°$. When applied to water droplets condensed onto a microgrooved aluminum surface, this method was shown to calculate the actual droplet volume to within 10% for 88% of the droplets analyzed; however, for droplets departing from the parallel-sided base contour shape, the aforementioned two-circle method provided more accurate results. The maximum contact angle for droplets on these surfaces, which occurs at $\phi = 90°$ due to the surface energy barrier to wetting imposed by the grooves, can also be predicted with a high level of accuracy using this new method. The measured contact angle at $\phi = 90°$ was predicted on average to within 2.9% for nonwetting (or composite) droplets and to within 6.6% for wetting droplets on these surfaces.

■ AUTHOR INFORMATION

Corresponding Author
*Phone: (513) 529-0718. Fax: (513) 529-0717. E-mail: sommerad@muohio.edu.

■ ACKNOWLEDGMENT

■ NOMENCLATURE

a_1, a_2, a_3 constants (eq 23)
A_c cross-sectional area (mm^2) (eq 15)
Bo Bond number ($\rho g D^2 \sin \alpha)/\gamma$
c_1, c_2 constants in the teardrop boundary profile (eq 5)
D_{eq} droplet equivalent diameter (mm)
g acceleration due to gravity (m s^{-2})
h droplet height (mm)
L half of a droplet's major axis (mm)
m droplet mass (mg)
r surface roughness factor (eq 2)

R_1 constant in the circular boundary profile (eq 6 and Figure 4)
V droplet volume (μL)
w half of a droplet's minor axis (mm), etched pillar width (μm)
x_h location where the droplet height is maximum (mm) (eq 23)
x_1, x_2, x_3 coordinates defined in Figure 4 (mm)
x, y, z coordinate directions

Greek Symbols
α surface inclination angle (deg)
β droplet aspect ratio, L/w
δ channel etch depth (μm), height of the circle's center (mm) (eq 6)
ϕ azimuthal angle (deg)
γ surface tension (N m^{-1})
φ surface area fraction used in the Cassie model (ratio of wetted surface area to projected area) (eq 3)
κ angle associated with the circular sector (deg) (Figure 4)
θ apparent contact angle (deg)
σ angle equal to $\theta_1 - \pi/2$ (deg) (eq 11)
ζ droplet base contour radius (mm)

Subscripts
adv advancing
eq equivalent
min minimum
max maximum
rec receding

■ REFERENCES

(1) Neumann, A. W.; Good, R. J. *J. Colloid Interface Sci.* **1972**, *38* (2), 341–358.
(2) Schwartz, L.; Garoff, S. *Langmuir* **1985**, *1*, 219–230.
(3) Oliver, J. F.; Huh, C.; Mason, S. G. *J. Adhes.* **1977**, *8*, 223–234.
(4) Morita, M.; Koga, T.; Otsuka, H.; Takahara, A. *Langmuir* **2005**, *21*, 911–918.
(5) Yoshimitsu, Z.; Nakajima, A.; Watanabe, T.; Hashimoto, K. *Langmuir* **2002**, *18*, 5818–5822.
(6) Narhe, R. D.; Beysens, D. A. *Phys. Rev. Lett.* **2004**, *93* (7), 076103.
(7) Chen, Y.; He, B.; Lee, J.; Patankar, N. A. *J. Colloid Interface Sci.* **2005**, *281*, 458–464.
(8) Dussan V., E. B.; Chow, R. T.-P. *J. Fluid Mech.* **1983**, *137*, 1–29.
(9) Dussan V., E. B. *J. Fluid Mech.* **1985**, *151*, 1–20.
(10) Dussan V., E. B. *J. Fluid Mech.* **1987**, *174*, 381–397.
(11) Briscoe, B. J.; Galvin, K. P. *Colloids Surf.* **1991**, *52*, 219–229.
(12) Brown, R. A.; Orr, F. M., Jr.; Scriven, L. E. *J. Colloid Interface Sci.* **1980**, *73* (1), 76–87.
(13) Extrand, C. W.; Kumagai, Y. *J. Colloid Interface Sci.* **1995**, *170*, 515–521.
(14) Dimitrakopoulos, P.; Higdon, J. J. L. *J. Fluid Mech.* **1999**, *395*, 181–209.
(15) Merte, H., Jr.; Son, S. *Wärme-Stoffübertrag.* **1987**, *21*, 163–168.
(16) Merte, H., Jr.; Yamali, C. *Wärme-Stoffübertrag.* **1983**, *17*, 171–180.
(17) Moy, E.; Cheng, P.; Policova, Z.; Treppo, S.; Kwok, D.; Mack, D. R.; Sherman, P. M.; Neumann, A. W. *Colloids Surf.* **1991**, *58*, 215–227.
(18) El Sherbini, A. I.; Jacobi, A. M. *J. Colloid Interface Sci.* **2004**, *273*, 556–565.
(19) El Sherbini, A. I.; Jacobi, A. M. *J. Colloid Interface Sci.* **2004**, *273*, 566–575.

(20) Amirfazli, A.; Graham-Eagle, J.; Pennell, S.; Neumann, A. W. *Colloids Surf., A* **2000**, *161*, 63–74.

(21) Bateni, A.; Susnar, S. S.; Amirfazli, A.; Neumann, A. W. *Colloids Surf., A* **2003**, *219*, 215–231.

(22) Li, W.; Amirfazli, A. *J. Colloid Interface Sci.* **2005**, *292*, 195–201.

(23) Antonini, C.; Carmona, F. J.; Pierce, E.; Marengo, M.; Amirfazli, A. *Langmuir* **2009**, *25* (11), 6143–6154.

(24) Young, T. In *Miscellaneous Works*; Peacock, G., Ed.; J. Murray: London, 1855; Vol. 1.

(25) Wenzel, T. N. *Ind. Chem. Eng.* **1936**, *28* (8), 988–994.

(26) Cassie, A. B. D.; Baxter, S. *Trans. Faraday Soc.* **1944**, *40*, 546–551.

(27) Sommers, A. D.; Jacobi, A. M. *J. Micromech. Microeng.* **2006**, *16* (8), 1571–1578.

(28) Sommers, A. D.; Jacobi, A. M. *J. Colloid Interface Sci.* **2008**, *328* (2), 402–411.